

# Integrability as a consequence of discrete holomorphicity: loop models

I T Alam<sup>1</sup> and M T Batchelor<sup>2,1,3</sup>

<sup>1</sup> Department of Theoretical Physics, Research School of Physics and Engineering, The Australian National University, Canberra ACT 0200, Australia

<sup>2</sup> Centre for Modern Physics, Chongqing University, Chongqing 400044, China

<sup>3</sup> Mathematical Sciences Institute, The Australian National University, Canberra ACT 0200, Australia

E-mail: Imam.Alam@anu.edu.au

E-mail: Murray.Batchelor@anu.edu.au

**Abstract.** In this paper, we explore the relationship between integrability and the discrete holomorphicity of a class of complex lattice observables in the context of the Potts dense loop model and the  $O(n)$  dilute loop model. It is shown that the conditions for integrability, namely, the inversion and Yang-Baxter relations, can be derived from the condition of holomorphicity of the observables. Furthermore, the  $Z$ -invariance of the models is shown to result in the invariance of the observables on the boundary of a sublattice under reshuffling of the rhombuses of its planar rhombic embedding.

## 1. Introduction

The celebrated rigorous proof of conformal invariance of the Ising model [1, 2] spurred renewed interest in the application of discrete complex analysis to two-dimensional critical lattice models. The approach has inspired mathematical proofs for a number of notable results in statistical physics. For the Ising model, these include the conformal invariance of spin correlations [3] and the energy density [4] and the existence of the scaling limit of domain walls [5]. For self-avoiding walks on the hexagonal lattice, proofs have been given for the connective constant [6] and the critical fugacity of surface adsorption [7, 8].

Of course, the solvability of these problems ought, ultimately, to be ascribed to the integrability [9] of the models. In a parallel development, it was discovered that a weakening of the condition of discrete holomorphicity, namely, imposing only the condition of vanishing discrete contour sum, is obeyed by a class of parafermionic observables on the lattice for a wide variety of models such as the Potts [10], the  $\mathbb{Z}_N$  [11] and the  $O(n)$  loop [12] models, both in the bulk [10, 11, 12] and with a boundary [13, 14]. Intriguingly, for these observables, the condition holds only on the integrable critical manifold of the Boltzmann weights, warranting a deeper understanding of the

connection between integrability and holomorphicity. In this paper, we refer to this weak form of holomorphicity only as discrete holomorphicity for simplicity.

Subsequently, we showed [15] that for Fateev-Zamolodchikov self-dual  $\mathbb{Z}_N$  models [16], discrete holomorphicity necessarily implies Yang-Baxter integrability conditions. In this paper, we demonstrate the generality of the connection by showing that analogous arguments hold for the loop models. The integrable structure in the cases considered here can alternatively be understood as arising from the quantum group [17] structure. In [18], the relevant parafermions were identified as non-local conserved currents [19] corresponding to this symmetry with their conservation law given by the condition of discrete holomorphicity. This approach leads directly to the Yang-Baxter equation by exploiting the associativity of the algebra. Our approach here, however, is focused on the connection with the  $Z$ -invariance [20] of these models. The holomorphic observable, remarkably, also has close connections [21] to the combinatorial approach [22] for the special case of the Ising model.

In section 2 we present our results for the critical Potts model in its dense loop formulation, that is, we derive the inversion relation and the Yang-Baxter equation from the condition of holomorphicity, and in section 3 we extend the results to the  $O(n)$  dilute loop model. In section 4 we present an alternative characterization of the observables which uses the  $Z$ -invariance of the model to define the observables on the boundary for the whole equivalence class of Baxter lattices sharing that boundary. Some concluding remarks are given in section 5.

## 2. The dense loop model

### 2.1. Yang-Baxter integrability

It is well-known [23, 24] that the  $N$ -state critical Potts model on a planar graph can be mapped to a dense loop model defined on its medial graph. We call a face of the covering graph (the planar dual of the medial graph) a plaquette and the edge of the original graph on which the plaquette is placed its axis. Each closed loop gets a statistical weight

$$n = \sqrt{N} = 2 \cos \lambda \quad (0 \leq N \leq 4, \quad 0 \leq \lambda \leq \frac{\pi}{2})$$

and each plaquette can have on it one of two configurations with weights  $a$  and  $b$  that depend on the interaction energy of its axis. We represent the  $R$ -matrix graphically as a formal linear combination of the configurations, or the connectivities, on the plaquette, which are essentially the 2 possible pairings between the 4 midpoints of the sides,

$$\begin{array}{c} \nearrow \\ \vee \\ \searrow \\ \alpha \end{array} = a_\alpha \begin{array}{c} \diamond \\ \text{---} \\ \text{---} \\ \text{---} \\ \text{---} \end{array} + b_\alpha \begin{array}{c} \diamond \\ \text{---} \\ \text{---} \\ \text{---} \\ \text{---} \end{array}$$

where  $\alpha$  is the spectral parameter with a normalization yet to be fixed. The axis connects two opposite corners of the plaquette, one of which is marked with a tag to track the orientation of the plaquette. For a rhombic embedding of the covering graph on the



**Figure 1.** The 5 different chord diagrams between 6 points that form the basis in the formal expansion of the Yang-Baxter equation.

plane, we call the angle at this corner the opening angle of the plaquette. For the model to be integrable, the weights must satisfy the Yang-Baxter equation

$$(1)$$

as well as the inversion relation,

$$(2)$$

The Temperley-Lieb algebra [25] allows formal expansion of the diagrams in the 5 possible connectivities, also known as chord diagrams, that correspond to the different pairings between 6 points (figure 1). In general, the number of pairings  $(2j)!/(j+1)j!$  of  $2j$  points on a circle by non-intersecting chords is known as the  $j^{\text{th}}$  Catalan number in combinatorics.

The resulting relations are

$$a_\alpha a_\beta a_\gamma = a_\alpha b_\beta b_\gamma + b_\alpha a_\beta b_\gamma + b_\alpha b_\beta a_\gamma + n b_\alpha b_\beta b_\gamma \quad (3)$$

$$a_\alpha b_{-\alpha} + b_\alpha a_{-\alpha} + n a_\alpha a_{-\alpha} = 0 \quad (4)$$

respectively, where the normalization of the spectral parameters is

$$\alpha + \beta + \gamma = 2\pi \quad (5)$$

suggesting a possible interpretation as angles.

## 2.2. The loop observable

A discretely holomorphic observable [10, 12] of the model, for a rhombic embedding of the covering lattice on the complex plane, is defined on the midpoint of the sides of the plaquettes,

$$\psi(z) = \sum_{\gamma \in \Gamma(z)} e^{-i\sigma W_\gamma(A, z)} w(\gamma)$$

Here  $\sigma$  is a real constant called the conformal spin of the observable,  $\Gamma(z)$  is the set of all the configurations having a curve, called the exploration path, between two fixed points

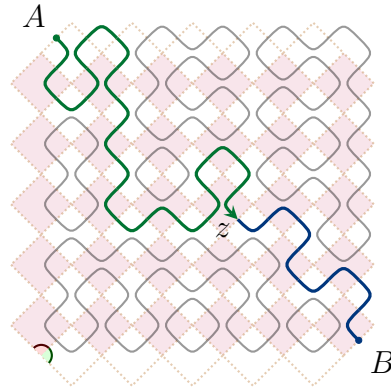


**Figure 2.** Contribution to the observable  $\psi(z)$  from a loop configuration on a regular square lattice. The thick curve is the exploration path that runs from  $A$  to  $B$  and has  $z$  lying on it. The shaded plaquettes correspond to the vertical, and the white plaquettes to the horizontal edges in the original Potts spin model. The marked angles at the lower left corner show that the opening angles of the two classes of rhombi are supplementary. The winding angle is the total angle that the curve turns to get from  $A$  to  $z$ , which, in this configuration, is zero.

$A$  and  $B$  on the boundary with  $z$  lying on it,  $w(\gamma)$  is the weight of the configuration  $\gamma$ , and  $W_\gamma(A, z)$  is the winding angle of the exploration path going from  $A$  to  $z$  (figure 2). That is, on each plaquette it obeys

$$\sum_{\diamond} \psi(z) \Delta z = 0$$

where the  $\Delta z$  are the differences in complex coordinates of the endpoints of the side  $z$  is on, traversed in the anticlockwise direction around the rhombus  $\diamond$ . Consequently such a sum around any closed path on the covering lattice vanishes to give a discrete analogue of Cauchy's integral theorem for holomorphic functions.

To establish the claim, Ikhlef and Cardy [12] considered the contour sum around a single rhombic plaquette with opening angle  $\alpha$ , breaking up the configuration into two parts for the interior and the exterior of the rhombus respectively, and grouping the terms by the exterior configuration, which thus for the purposes of the argument can be thought of as frozen henceforth, and then by the point of first entry into the rhombus for the curve. Therefore it suffices for the sum to vanish for each of these groupings individually. Defining an auxiliary function

$$\phi(\alpha) = e^{i(1-\sigma)\alpha}$$

for notational convenience, we have, for the two possible connectivities of the external configurations (figure 3),

$$n (1 - \phi(\alpha - \pi)) a_\alpha + (1 - \phi(\alpha - \pi) + \phi(-\pi) - \phi(\alpha)) b_\alpha = 0 \quad (6)$$

$$(1 - \phi(\alpha - \pi) + \phi(\pi) - \phi(\alpha)) a_\alpha + n (1 - \phi(\alpha)) b_\alpha = 0 \quad (7)$$

For non-trivial solutions to exist, the determinant of the system must vanish, and we take the factors of the determinant independent of  $\alpha$  to be zero, so that the condition

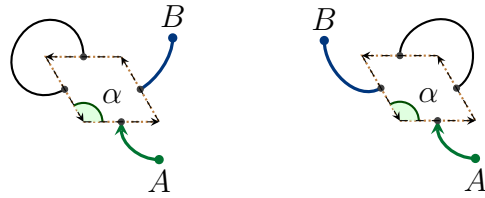


**Figure 3.** The external configurations for equations (6) and (7) respectively. The discrete contour consisting of the  $\Delta z$  is indicated by dashed arrows.

is satisfied on all rhombuses, to obtain

$$n^2 - 2 = \phi(\pi) + \phi(-\pi)$$

and therefore,

$$1 - \sigma = \frac{2\lambda}{\pi} - 2\ell \quad (\ell \in \mathbb{Z})$$

which results in a family of solutions labelled by an integer  $\ell$ ,

$$\frac{a_\alpha}{b_\alpha} = (-1)^\ell \frac{\sin\left(\left(\frac{\lambda}{\pi} - \ell\right)\alpha\right)}{\sin\left(\left(\frac{\lambda}{\pi} - \ell\right)(\pi - \alpha)\right)}$$

all of which satisfy the integrability condition as shown below. The standard solution  $a = \sin u$ ,  $b = \sin(\lambda - u)$  corresponds to  $\ell = 0$ , and lets us identify the angle, in this case, as a (re-scaled) spectral parameter,

$$u = \frac{\lambda}{\pi} \alpha$$

It was observed long ago [26] that this is the required embedding of the anisotropic lattice for correlations to be conformally, or more simply, rotationally, invariant. The criticality condition

$$\frac{a_{\pi-\alpha}}{b_{\pi-\alpha}} \frac{a_\alpha}{b_\alpha} = 1$$

can be immediately verified, and enables the identification of these supplementary weights to be the dual weights in the other lattice direction (figure 2). Thus the role of the crossing parameter is played by  $\pi$  in this normalization.

It is instructive to compare, once a suitable observable has been identified, the problem of solving the discrete holomorphicity condition which is linear in the weights with a given spectral parameter, with the usual one of finding a solution of the Yang-Baxter equation which is cubic in the weights and relates weights with different spectral parameters.

### 2.3. Rhombic embeddings of Baxter lattices

The appearance of rhombic embeddings, or equivalently, isoradial embeddings, in the above construction is doubly propitious, as on one hand, discrete complex analysis on them is natural [27], and on the other hand, the key class of lattices for integrable models [20], usually called the Baxter lattices, admits such embeddings [28]. Our argument

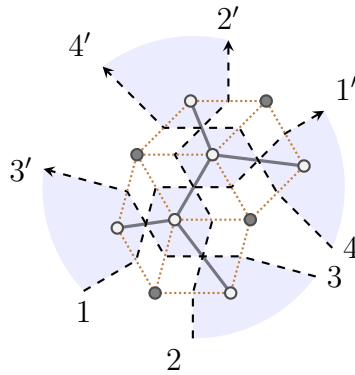


**Figure 4.** Part of a Baxter lattice with its rhombic embedding. The rapidity lines are dashed. One of the bipartite classes of regions is shaded. The spins are on the white circles, and the disorder variables are on the shaded circles. The thick lines are edges indicating interaction between spins. The dotted lines show the associated rhombic embedding with each rhombus having an interaction edge as a diagonal that we call its axis.

draws from related ideas that have appeared in geometrical characterization of Baxter lattices [29], and emergence of discrete conformal symmetry in solutions of the star-triangle relation [30].

We start, therefore, with a Baxter lattice (figure 4). It is a planar graph defined by a set of directed lines called rapidity lines, which are usually straight, but for our purposes it is only necessary to keep the topological characterization: no line crosses itself or is periodic, and no two lines cross each other more than once. The lines divide the plane into bipartite regions, and for spin models such as the Potts model, we place spins, which are the nodes of the graph, on one class of regions, and disorder variables, which are the faces of the graph, on the other class. At each crossing of rapidity lines, where four regions of alternating classes meet, an edge connects the two spins to indicate interaction between them. If we place a parameter, called the rapidity parameter, on each line, then the interaction on an edge can depend on the difference, called the spectral parameter, of the parameters of the two crossing lines.

The covering lattice of this graph is a quad-graph whose nodes are the spins and the disorder variables, and these are connected by an edge if the two containing regions are adjacent, so each edge connects a spin with a disorder variable. Each face then has as one diagonal an edge of the original lattice which we call the axis. In the terminology of [28], a train-track is a sequence of adjacent faces of a quad-graph which upon entering a face via an edge exits through the opposite edge, and a quad-graph has a rhombic embedding if and only no train-track crosses itself or is periodic, and no two train-tracks cross each other more than once. The identification of train-tracks with rapidity lines is thus immediate, and since in a rhombic embedding all the edges that cross a rapidity line are parallel, we can identify (the complex exponential of the imaginary unit times) the rapidity parameter with the common direction, called the transversal, of the edges, treated as a unimodular complex number. The spectral parameter is

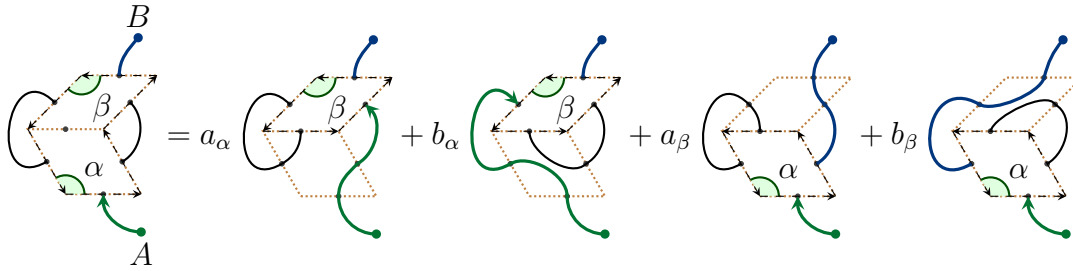


**Figure 5.** The contour sum around two rhombuses. The dashed arrows show the discrete contours. The labels on the endpoints of the curve on the right hand side has been omitted for clarity.

then naturally given by the angle between the two transversals of a rhombus, or its supplement, depending on the direction of crossing and the placement of the axis. Since the common length of the sides of all the rhombus provide the only length scale of the problem, we set it to unity without loss of generality.

The conditions of integrability, that is, the Yang-Baxter equation (1) and the inversion relation (2), ensure that the partition function of a Baxter lattice remains unchanged, or possibly acquires a trivial constant factor, as the rapidity lines are moved around topologically, that is, by the third and the second Reidemeister moves respectively, while the end points of the lines are kept fixed. This property is referred to as  $Z$ -invariance in the literature. In other words, the partition function is a function only of the permutation (denoted by primes in figure 4), or more generally, the braiding, of the rapidity lines, and is independent of the internal lattice. Our identification of rapidity parameters and transversals implies that the boundary of the rhombic domain remains unchanged by such moves, and the boundary can thus be regarded as belonging to the equivalence class of such lattices.

#### 2.4. Derivation of integrability

The proof of discrete holomorphicity of the observable by grouping terms by external connectivities suggests a natural extension to any simply-connected domain of rhombic faces. A simple proof is given by induction on the number of faces, and proceeds by dividing the domain into smaller pieces, and regarding all but one of the pieces as part of the external configuration.

To illustrate the procedure, we take the domain to consist of two rhombuses (figure 5), having opening angles  $\alpha$  and  $\beta$ , with an external connectivity of chord diagram  $V$  (figure 1). The figure denotes the discrete contour sum of the observable around the shown contour, which can be broken up into contour sums around each rhombus. We then expand the external rhombus into its connectivities. Evidently, the total sum reduces to a linear combination of sums around only one rhombus, all of which are known to vanish, regardless of the entry points. Therefore, the total sum itself vanishes for the given external configuration. We thus conclude that the discrete contour sum of

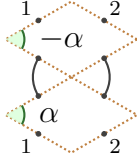


**Figure 6.** A pair of ghost rhombuses. The internal unnamed points connected by the thick lines are identified. The external numbered points on the plane are also identified, allowing the pair to be folded up.

the observable around any simply-connected domain vanishes for each of the external connectivities individually.

Evaluating the left hand side of figure 5 directly, that is, setting the contour sum of the observable around two rhombuses with the external chord diagram V to zero, we arrive at

$$(\phi(\pi - \beta) - \phi(\alpha - \pi)) n^2 a_\alpha a_\beta + (\phi(-\beta) - \phi(\alpha)) n^2 b_\alpha b_\beta \\ + (\phi(\pi - \beta) + \phi(-\beta) - \phi(\alpha) - \phi(\alpha - \pi)) (n a_\alpha b_\beta + n b_\alpha a_\beta) = 0$$

which is quadratic in the weights. Putting  $\beta = -\alpha$  gives

$$(\phi(\pi + \alpha) - \phi(\alpha - \pi)) n (n a_\alpha a_{-\alpha} + a_\alpha b_{-\alpha} + b_\alpha a_{-\alpha}) = 0$$

from which we immediately conclude that

$$a_\alpha b_{-\alpha} + b_\alpha a_{-\alpha} + n a_\alpha a_{-\alpha} = 0$$

that is, the inversion relation (2) holds.

It is interesting to note that the inversion relation is at odds with the premises of the rhombic embedding theorem in that the two rapidity lines cross twice, and hence, the relation does not admit an embedding, in contrast to the Yang-Baxter equation below. However, the appearance of the negative angle, or equivalently, the negative area, may be interpreted as the result of flipping a plaquette over to reveal another from underneath (figure 6), whose contributions to the weight of the configuration cancel. Also, with this interpretation, the four external midpoints are, in fact, superposed to give just two midpoints on adjacent sides, perhaps on some other rhombus, and therefore the relation permits the insertion of a pair of rhombuses with opposite angles at will, as in the standard proof of commuting transfer matrices. We also note that such topological modifications to the Baxter lattice respect the  $Z$ -invariance, or the invariance of the partition function, and can serve to broaden the equivalence class of lattices having the same embedding, once such ghost pairs of rhombuses are allowed.

To prove the Yang-Baxter relation, we consider a third rhombus with opening angle  $\gamma$  to complete the hexagon, resulting in the geometric requirement, equation (5), that relates the spectral parameters. Again, evaluating the contour sum of the observable around the hexagon (figure 7) for external chord diagram V, we get

$$(\phi(-\beta) - \phi(\alpha)) n^2 \text{YB}(\alpha, \beta, \gamma) = 0$$



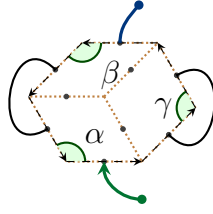


**Figure 7.** The hexagon formed by three rhombuses with opening angles that sum up to  $2\pi$ . The contour sum is around the rhombus with a particular external chord diagram that produces the Yang-Baxter equation directly.

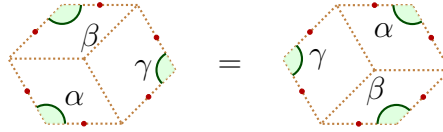


**Figure 8.** The two ways to tile the hexagon with three rhombuses. For the Potts spin model, the left arrangement makes a star, and the right makes a triangle of interaction edges, and so we refer to the two arrangements as such. The dots mark the observables on the boundary.

where we have defined

$$\text{YB}(\alpha, \beta, \gamma) := b_\alpha b_\beta a_\gamma + b_\alpha a_\beta b_\gamma + a_\alpha b_\beta b_\gamma + n b_\alpha b_\beta b_\gamma - a_\alpha a_\beta a_\gamma$$

with the understanding that the angles follow equation (5) so that there are really two independent variables. Therefore we immediately conclude that

$$\text{YB}(\alpha, \beta, \gamma) = 0$$

or in other words, equation (3) holds. Here, and in what follows, including the appendix, we avoid special treatment of isolated values of  $n$  for which the proofs can be adopted, or an appeal to continuity can be made.

However, in light of the result to follow in section 4, we have an alternate proof by considering the two different arrangements of the rhombuses to produce the same hexagon (figure 8). For each of the external connectivities (figure 1), we take the contour sum of the two sides, and take the difference. Since both of the sums vanish, so does the difference, and thus we have

$$\begin{aligned} (n \phi(\alpha - 2\pi) - n \phi(\alpha) + n^3 \phi(-\beta) - n^3) \text{YB}(\alpha, \beta, \gamma) &= 0 \\ n^2(\phi(-\beta) - \phi(2\pi - \beta)) \text{YB}(\alpha, \beta, \gamma) &= 0 \\ n^2(\phi(\alpha - 2\pi) - \phi(\alpha)) \text{YB}(\alpha, \beta, \gamma) &= 0 \\ (n^3 - n \phi(2\pi - \beta) + n \phi(-\beta) - n^3 \phi(\alpha)) \text{YB}(\alpha, \beta, \gamma) &= 0 \\ 2n^2(\phi(-\beta) - \phi(\alpha)) \text{YB}(\alpha, \beta, \gamma) &= 0 \end{aligned}$$

for all  $\alpha$  and  $\beta$ , and therefore all of them show that the Yang-Baxter equation, or the star-triangle relation, holds.

### 3. The dilute loop model

#### 3.1. Yang-Baxter integrability

The dilute, or  $O(n)$ , loop model arises as the high-temperature expansion of an  $n$ -component vector spin model on the plane that is invariant under the action of the rotation group. In this model, each closed loop has a fugacity, or weight

$$n = -2 \cos 4\eta \quad (-2 \leq n \leq 2, \quad 0 \leq \eta \leq \frac{\pi}{4})$$

and the weights of the configurations on the plaquettes are encoded in the  $R$ -matrix as a linear combination of the 9 connectivities between 4 points, where the non-intersecting curves are allowed to be absent, with

$$\begin{array}{c} \swarrow \quad \nearrow \\ \searrow \quad \nwarrow \\ \alpha \end{array} = t_\alpha \begin{array}{c} \diamond \\ \diamond \end{array} + u_{1\alpha} \left( \begin{array}{c} \circ \\ \circ \end{array} + \begin{array}{c} \circ \\ \circ \end{array} \right) + u_{2\alpha} \left( \begin{array}{c} \smile \\ \smile \end{array} + \begin{array}{c} \frown \\ \frown \end{array} \right) + v_\alpha \left( \begin{array}{c} \diagdown \\ \diagup \end{array} + \begin{array}{c} \diagup \\ \diagdown \end{array} \right) + a_\alpha \begin{array}{c} \circ \\ \circ \end{array} + b_\alpha \begin{array}{c} \circ \\ \circ \end{array}$$

The configurations where a curve starts or ends abruptly in the bulk are not allowed and can be assigned a null weight. The generality sacrificed in favour of brevity in the choice of the weights is ultimately justified by the obtained solutions.

Expanding the Yang-Baxter equation (1) in this  $R$ -matrix, we get 51 inequivalent connectivities between 6 points and their corresponding equations, which reduce to

$$\text{YB}_1(\alpha, \beta, \gamma) := u_{2\alpha} u_{2\beta} a_\gamma + n u_{2\alpha} u_{2\beta} b_\gamma + t_\alpha t_\beta u_{2\gamma} - u_{1\alpha} u_{1\beta} t_\gamma - v_\alpha v_\beta u_{2\gamma} = 0$$

$$\text{YB}_2(\alpha, \beta, \gamma) := t_\alpha u_{1\beta} v_\gamma + u_{2\alpha} v_\beta u_{1\gamma} - t_\gamma u_{1\beta} v_\alpha - u_{1\alpha} v_\beta u_{2\gamma} = 0$$

$$\text{YB}_3(\alpha, \beta, \gamma) := u_{2\alpha} b_\beta a_\gamma + u_{2\alpha} a_\beta b_\gamma + n u_{2\alpha} b_\beta b_\gamma + t_\alpha u_{2\beta} u_{2\gamma} - a_\alpha u_{1\beta} u_{1\gamma} = 0$$

$$\text{YB}_4(\alpha, \beta, \gamma) := v_\alpha u_{1\beta} b_\gamma + u_{1\alpha} v_\beta u_{2\gamma} - a_\alpha u_{1\beta} v_\gamma = 0$$

$$\text{YB}_5(\alpha, \beta, \gamma) := u_{1\alpha} b_\beta u_{1\gamma} + v_\alpha u_{2\beta} v_\gamma - a_\alpha u_{2\beta} a_\gamma = 0$$

$$\text{YB}_6(\alpha, \beta, \gamma) := b_\alpha b_\beta a_\gamma + b_\alpha a_\beta b_\gamma + a_\alpha b_\beta b_\gamma + n b_\alpha b_\beta b_\gamma + u_{2\alpha} u_{2\beta} u_{2\gamma} - a_\alpha a_\beta a_\gamma = 0$$

subject to equation (5), upon permuting  $\alpha$ ,  $\beta$  and  $\gamma$ . We will refer to the functions defined, which we need to show to vanish, as the  $\text{YB}_i(\alpha, \beta, \gamma)$  functions. In general, the number of ways of drawing non-intersecting chords on a circle between  $j$  points,  $\sum_{k=0}^{\lfloor j/2 \rfloor} \binom{j}{2k} (2j)! / (j+1)! j!$ , is known as the  $j^{\text{th}}$  Motzkin number in combinatorics. Here 51 is the  $6^{\text{th}}$  Motzkin number.

#### 3.2. The loop observable

The holomorphic observable [12] of the model is defined on the midpoints of the sides of the plaquettes to be

$$\psi(z) = \sum_{\gamma \in \Gamma(z)} e^{-i \sigma W_\gamma(A, z)} w(\gamma)$$

where  $\Gamma(z)$  now is the set of configurations that have an open path from  $A$  to  $z$ , which is the exploration path for this case, and the rest of the symbols are analogous to those in the dense loop model. Again, we want

$$\sum_{\diamond} \psi(z) \Delta z = 0$$

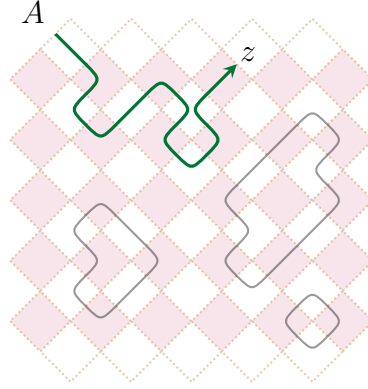


**Figure 9.** Contribution to the loop observable  $\psi(z)$  for a configuration  $\gamma$  on a regular square lattice. The winding angle  $W_\gamma(A, z)$  is the total angle the exploration path turns to get from the boundary point  $A$  to the specified point  $z$ , which in this figure is  $\pi/2$ .

on a rhombus of opening angle  $\alpha$ , and to this end, we consider grouping the terms by the specific point through which the path enters the plaquette. With one point already accounted for, the remaining 3 points can have 4 connectivities (the 3<sup>rd</sup> Motzkin number), and consequently, we have the discrete holomorphicity relations as in [12],

$$t_\alpha - \phi(\alpha - \pi) u_{1\alpha} - \phi(\alpha) u_{2\alpha} - v_\alpha = 0 \quad (8)$$

$$\phi(\pi) u_{1\alpha} + n u_{2\alpha} + \phi(\alpha - 2\pi) v_\alpha - \phi(\alpha) a_\alpha - n \phi(\alpha) b_\alpha = 0 \quad (9)$$

$$\phi(\alpha + \pi) u_{1\alpha} + \phi(\alpha - 2\pi) u_{2\alpha} + n v_\alpha - \phi(2\pi) a_\alpha - \phi(-2\pi) b_\alpha = 0 \quad (10)$$

$$n u_{1\alpha} + \phi(-\pi) u_{2\alpha} + \phi(\alpha + \pi) v_\alpha - n \phi(\alpha - \pi) a_\alpha - \phi(\alpha - \pi) b_\alpha = 0 \quad (11)$$

with the same definition of  $\phi(\alpha)$  as before. Considering the other points the curve could enter through, we find that the complex conjugates of the equations are also satisfied, which ensures that the weights are real. Consequently we have 8 real equations for 6 real variables, but fortunately 2 of them are superfluous, and the system has non-trivial solutions when the determinant of the reduced system vanishes, a condition that we ensure by choosing the  $\alpha$  independent factor to be zero, which results in

$$\phi(4\pi) + \phi(-4\pi) = 3n - n^3$$

so that

$$1 - \sigma = \frac{3\eta}{\pi} + \frac{1}{2}\ell \quad (\ell \in \mathbb{Z})$$

Thus we again find a series of solutions to the integrability conditions labelled by an integer  $\ell$ , as is proved below. However, for clarity, we restrict ourselves in this section to the  $\ell = 0$  case, for which the solution is

$$t_\alpha = \sin \frac{3\eta}{\pi} \alpha \sin \frac{3\eta}{\pi} (\pi - \alpha) + \sin 2\eta \sin 3\eta$$

$$u_{1\alpha} = \sin \frac{3\eta}{\pi} \alpha \sin 2\eta$$

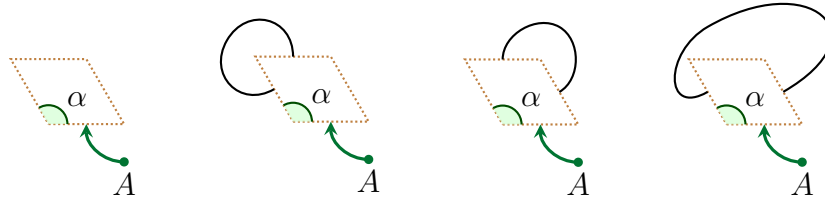


**Figure 10.** The external configurations for equations (8), (9), (10), and (11) respectively. The embedding of the external curves must be so that they do not enclose the point  $A$  on the boundary, which uniquely specifies the winding angles.

$$\begin{aligned}
 u_{2\alpha} &= \sin \frac{3\eta}{\pi} (\pi - \alpha) \sin 2\eta \\
 v_{\alpha} &= \sin \frac{3\eta}{\pi} \alpha \sin \frac{3\eta}{\pi} (\pi - \alpha) \\
 a_{\alpha} &= \sin \frac{3\eta}{\pi} \alpha \sin \left( \frac{3\eta}{\pi} \alpha - \eta \right) \\
 b_{\alpha} &= \sin \frac{3\eta}{\pi} (\pi - \alpha) \sin \left( \frac{3\eta}{\pi} (\pi - \alpha) - \eta \right)
 \end{aligned}$$

which is indeed the standard solution [31], with

$$u = \frac{3\eta}{\pi} \alpha$$

Note that the convexity requirement on the rhombuses,  $0 < \alpha < \pi$ , guarantees positivity of the weights for the  $\ell = 0$  solution, for both the dilute and the dense loop models. Also, it is reasonable to expect that with a square lattice with anisotropic interaction, the correlation functions will become rotationally invariant when it is embedded on the plane according to this prescription for the angles.

It is interesting to note that the existence of discretely holomorphic observables indicate an explanation of the fact that solvable critical weights are usually trigonometric. Since the real weights have to obey homogeneous linear relations with coefficients that are sums of pure complex phases, their solutions are real-valued rational functions of those phases, and thus trigonometric functions are the most natural candidates. This provides a strong motivation to look for such observables in critical solvable models which are known to have trigonometric weights, especially those with their continuum limits described by minimal models.

### 3.3. Derivation of integrability

The extension of the vanishing contour sum property to simply-connected domains with specified external configuration applies *mutatis mutandis* to the dilute model. We therefore consider figure 8 in this context where the curve enters via a specified point, say, the base. The remaining 5 points may have 21 connectivities (the 5<sup>th</sup> Motzkin number), and the resulting equations, which are the differences of the contour sums around the hexagon for the two arrangements, are omitted for brevity. However, in

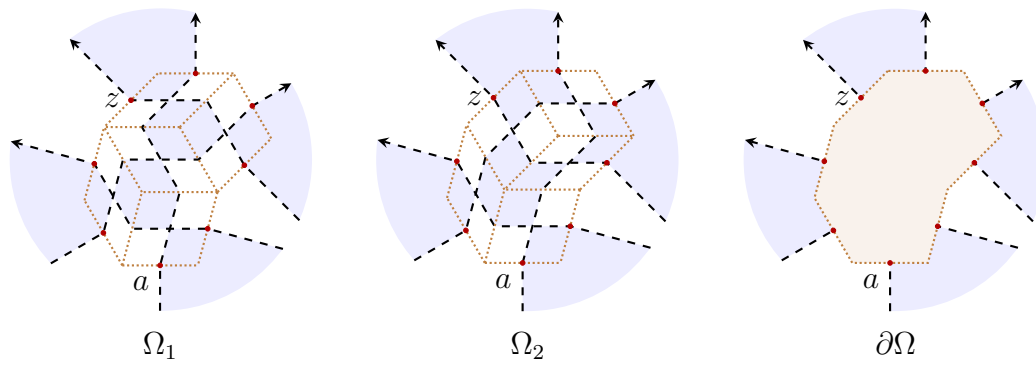


**Figure 11.** Two equivalent Baxter sublattices,  $\Omega_1$  and  $\Omega_2$ , and their common boundary  $\partial\Omega$ . The highlighted points are the midpoint of the sides of the rhombuses that are on  $\partial\Omega$ . The exploration path first enters the sublattice via the boundary point  $a$ . The value of the observable at a boundary point  $z$  remains the same for the two lattices and unambiguously defines it on  $\partial\Omega$  without referring to the interior.

these equations, the weights enter only through the  $YB_i(\alpha, \beta, \gamma)$  functions. They are therefore an over-determined linear system in the functions that in fact, as shown in the Appendix, forces them to vanish, proving the Yang-Baxter relations.

#### 4. Invariance of the observable at the boundary

Once the integrability conditions are derived from the holomorphicity condition, however, an alternative explanation of the proof can be deduced. Inside a Baxter lattice, we consider a sublattice  $\Omega_1$ , and modify it by Reidemeister moves of the rapidity lines that leave the exterior of the sublattice unaltered (figure 11), to obtain another sublattice  $\Omega_2$ . With our identification of rapidity parameters with transversals in section 2.3, the boundary of the sublattices in a rhombic embedding remains the same, and we denote it by  $\partial\Omega$ . The effect of the modifications on the embedding is to shuffle rhombuses around, as is evident from figure 8.

Now compare, for the two sublattices, the observable at a midpoint  $z$  on  $\partial\Omega$ ,

$$\psi_{\Omega}(z) = \sum_{a \in \partial\Omega} \left( \sum_{\gamma \in \Gamma_{\Omega}(z;a)} e^{-i\sigma W_{\gamma}(A,z)} w(\gamma) \right)$$

where  $\Omega$  stands for either of the two sublattices, and  $\Gamma_{\Omega}(z;a)$  is the subset of  $\Gamma_{\Omega}(z)$  for which  $a$  is the point of entry of the exploration path into the interior. Clearly, it suffices to show that the quantity in parentheses is equal for the two sublattices to prove that

$$\psi_{\Omega_1}(z) = \psi_{\Omega_2}(z)$$

and consequently, for every member of the equivalence class of the sublattices, and hence,  $\psi$  is unambiguously defined on  $\partial\Omega$ , independent of its interior lattice structure.

The exterior common to the two sublattices can be factored out by grouping the terms by the configurations on it, which fixes the value of the winding angle up to  $a$ , and thus can be factored out. The only information we need about this configuration

is then its connectivity given by a chord diagram appropriate for the model, which we refer to as the external chord diagram. Note that for the dilute model, the diagrams that connect  $a$  to another point on  $\partial\Omega$  are not allowed as external diagrams.

Hence we are left with comparing, for the two sublattices,

$$\sum_{\gamma \in \Gamma_{\Omega}^{\text{int}}(z;a)} e^{-i \sigma W_{\gamma}(a,z)} w(\gamma)$$

where a given external diagram is imposed. Here  $\Gamma_{\Omega}^{\text{int}}(z;a)$  is the set of interior configurations on the sublattice  $\Omega$  where  $z$  and  $a$  lie on the same curve, possibly going through both the interior and the exterior of the sublattice. This time we group the terms in the sum by the internal chord diagrams, that is, the connectivity between the points on  $\partial\Omega$  in the internal configurations, for the comparison. For each group, the winding angles are the same because the curve follow identical chords on both of the chord diagrams which, by the existence of the common boundary  $\partial\Omega$ , have well-defined winding angles for each segment of the curve joining two points on it.

The quantity left to compare is the sums of weights of all configurations with the same chord diagrams for the two sublattices. Since the external and internal chord diagrams together determine the number of closed loops between them, this is equivalent to comparing the partition functions of the two lattices, which are identical due to the  $Z$ -invariance guaranteed by the integrability conditions already proven. Note that even though not all of the configurations in the definition of the observable in the dilute loop model is allowed in the partition function, the internal configurations are all allowed since the open path ends on its boundary.

We thus have the invariance of the observable on the boundary under Reidemeister moves of the rapidity lines inside, or equivalently, local reshuffling of rhombuses in the embedding. This provides another characterization of the observables besides discrete holomorphicity. It is interesting to note that discrete holomorphicity then provides linear relations among partition functions with different chord diagrams on the same lattice, whereas the integrability conditions show the equality of partition functions with the same chord diagram on different lattices. Of course, for just one rhombus, the partition functions with different chord diagrams are just the Boltzmann weights themselves.

## 5. Conclusion

In summary, discrete holomorphicity of the observables, on simply-connected domains tiled by convex rhombuses, generates linear equations between the partition functions with different internal connectivities of the boundary points. For one rhombus, these are linear equations in the weights, which are solved by finding the conformal spin by setting the determinant of the system of equations to zero. For two rhombuses, these equations are quadratic in the weights, and imply the inversion relation. For three rhombuses, they imply the Yang-Baxter relation. In general, for a domain with  $k$  rhombuses, the linear equation is among degree  $k$  homogeneous polynomials in the weights. With the

integrability conditions satisfied, the  $Z$ -invariance of the models defines the observable on the boundary of the domain for the equivalence class of Baxter lattices.

We note, however, that unlike the case of Cauchy's integral formula,

$$\psi(z_0) = \frac{1}{2\pi i} \oint_{\partial\Omega} \frac{\psi(z)}{z - z_0} dz$$

the values of the observable on the boundary do not uniquely specify the values in the interior. As was explained in [32], this is because the number of variables, that is the number of midpoints of the sides of the rhombuses, far exceeds the number of equations, that is, one equation of holomorphicity per rhombus. The observable defined on the Ising model [1], of course, is the glaring exception.

## Acknowledgments

We thank John Cardy for his invaluable guidance and kind hospitality in Oxford. We also thank Vladimir Bazhanov for his inspirations and insights, and Yvan Saint-Aubin, Jan de Gier, Alexander Lee and Rodney Baxter for helpful discussions. We thank the Rudolf Peierls Centre for Theoretical Physics for their hospitality during our visits to Oxford. MTB particularly thanks All Souls College for support through a Visiting Fellowship. He also acknowledges support from the 1000 Talents Program of China and from Chongqing University. This work has also been supported by the Australian Research Council through grant DP130102839.

## Appendix

In this section, we show that the vanishing differences of the discrete contour sums around the hexagon with the two arrangements, the star and the triangle, for the 21 different connectivities, imply the Yang-Baxter equations for the dilute loop model discussed in section 3.1. Of the equations, the following subset suffices,

$$\begin{aligned} \phi(\alpha) (\text{YB}_4(\alpha, \gamma, \beta) - n\text{YB}_4(\beta, \gamma, \alpha)) + n\text{YB}_2(\alpha, \beta, \gamma) - \phi(\pi)\text{YB}_1(\alpha, \gamma, \beta) \\ + \phi(\alpha + \pi)\text{YB}_3(\gamma, \alpha, \beta) - \phi(\alpha - 3\pi)\text{YB}_5(\alpha, \gamma, \beta) = 0 \end{aligned} \quad (\text{A.1})$$

$$\begin{aligned} \phi(\alpha - \pi) (\text{YB}_4(\beta, \gamma, \alpha) - n\text{YB}_4(\alpha, \gamma, \beta)) + \phi(\alpha) (\text{YB}_5(\alpha, \gamma, \beta) - n\text{YB}_3(\gamma, \alpha, \beta)) \\ + n\text{YB}_1(\alpha, \gamma, \beta) + \phi(-\pi)\text{YB}_2(\gamma, \beta, \alpha) = 0 \end{aligned} \quad (\text{A.2})$$

$$\begin{aligned} \phi(-\beta)\text{YB}_1(\alpha, \gamma, \beta) - \phi(\alpha)\text{YB}_1(\beta, \gamma, \alpha) + \phi(\pi - \beta)\text{YB}_2(\alpha, \beta, \gamma) \\ + \phi(\alpha - \pi)\text{YB}_2(\gamma, \alpha, \beta) = 0 \end{aligned} \quad (\text{A.3})$$

$$\begin{aligned} \phi(\pi - \beta) (n\text{YB}_4(\beta, \gamma, \alpha) - \text{YB}_4(\alpha, \gamma, \beta)) + \phi(-\beta) (n\text{YB}_3(\gamma, \alpha, \beta) - \text{YB}_5(\alpha, \gamma, \beta)) \\ - n\text{YB}_1(\beta, \gamma, \alpha) + \phi(\pi)\text{YB}_2(\beta, \alpha, \gamma) = 0 \end{aligned} \quad (\text{A.4})$$

$$\begin{aligned} \phi(-\beta) (n\text{YB}_4(\alpha, \gamma, \beta) - \text{YB}_4(\beta, \gamma, \alpha)) + n\text{YB}_2(\gamma, \alpha, \beta) + \phi(-\pi)\text{YB}_1(\beta, \gamma, \alpha) \\ - \phi(-\beta - \pi)\text{YB}_3(\gamma, \alpha, \beta) + \phi(3\pi - \beta)\text{YB}_5(\alpha, \gamma, \beta) = 0 \end{aligned} \quad (\text{A.5})$$

$$\begin{aligned} \phi(\alpha) (1 - n^2) \text{YB}_6(\alpha, \beta, \gamma) + n^2\text{YB}_3(\alpha, \beta, \gamma) - n\text{YB}_5(\beta, \alpha, \gamma) \\ + \phi(2\pi - \beta) (n\text{YB}_5(\alpha, \gamma, \beta) - \text{YB}_3(\gamma, \alpha, \beta)) \end{aligned}$$

$$\begin{aligned}
& + \phi(-\beta - \pi) (n\text{YB}_4(\alpha, \gamma, \beta) - \text{YB}_4(\beta, \gamma, \alpha)) \\
& + \phi(-\pi) (n\text{YB}_4(\beta, \alpha, \gamma) - \text{YB}_4(\gamma, \alpha, \beta)) = 0
\end{aligned} \tag{A.6}$$

In addition, to utilize the symmetries of the  $\text{YB}_i$  functions, we make the following replacements whenever the left hand sides occur in the calculations,

$$\begin{aligned}
\text{YB}_2(\gamma, \beta, \alpha) &\rightarrow -\text{YB}_2(\alpha, \beta, \gamma) & \text{YB}_2(\gamma, \alpha, \beta) &\rightarrow -\text{YB}_2(\beta, \alpha, \gamma) \\
\text{YB}_5(\beta, \gamma, \alpha) &\rightarrow \text{YB}_5(\alpha, \gamma, \beta) & \text{YB}_3(\gamma, \beta, \alpha) &\rightarrow \text{YB}_3(\gamma, \alpha, \beta)
\end{aligned}$$

We ignore isolated points for the values of  $n$  to keep the proof general, although the special cases can be handled similarly, or using the continuity of the YB functions and the weights. We start by multiplying equation (A.1) by  $\phi(-\pi)$  to express  $\text{YB}_1$  in terms of the others, enabling us to eliminate its subsequent occurrences,

$$\begin{aligned}
\text{YB}_1(\alpha, \gamma, \beta) &= n\phi(-\pi)\text{YB}_2(\alpha, \beta, \gamma) - n\phi(\alpha - \pi)\text{YB}_4(\beta, \gamma, \alpha) \\
& + \phi(\alpha)\text{YB}_3(\gamma, \alpha, \beta) + \phi(\alpha - \pi)\text{YB}_4(\alpha, \gamma, \beta) - \phi(\alpha - 4\pi)\text{YB}_5(\alpha, \gamma, \beta)
\end{aligned}$$

so that equation (A.2) gives, after multiplication by  $\phi(\pi - \alpha)/(n^2 - 1)$ , an expression for  $\text{YB}_4$ ,

$$\begin{aligned}
\text{YB}_4(\beta, \gamma, \alpha) &= \frac{1}{n^2 - 1} \left( n^2\phi(-\alpha)\text{YB}_2(\alpha, \beta, \gamma) + \phi(-\alpha)\text{YB}_2(\gamma, \beta, \alpha) \right. \\
& \left. - (n\phi(-3\pi) - \phi(\pi))\text{YB}_5(\alpha, \gamma, \beta) \right)
\end{aligned}$$

We now multiply by  $(n + 1)$  and substitute  $\text{YB}_1$  and  $\text{YB}_4$  into equations (A.3), (A.4), and (A.5) successively, to get

$$\begin{aligned}
& (-\phi(\alpha - \beta) - \phi(\alpha - \beta - 4\pi) + \phi(\alpha + \beta) + \phi(\alpha + \beta - 4\pi))\text{YB}_5(\alpha, \gamma, \beta) \\
& - (n + 1)(\phi(\alpha - \pi) - \phi(\alpha - 2\beta - \pi))\text{YB}_2(\beta, \alpha, \gamma) \\
& + (n + 1)(\phi(\pi - \beta) - \phi(\beta - \pi))\text{YB}_2(\alpha, \beta, \gamma) \\
& + (n + 1)(\phi(\alpha - \beta) - \phi(\alpha + \beta))\text{YB}_3(\gamma, \alpha, \beta) = 0
\end{aligned} \tag{A.7}$$

$$\begin{aligned}
& (\phi(2\pi - \beta) - \phi(-\beta) - n\phi(-\beta - 2\pi) - n\phi(-\beta) + n\phi(\beta) + n\phi(\beta - 4\pi))\text{YB}_5(\alpha, \gamma, \beta) \\
& + (n + 1)(\phi(\pi) - \phi(\pi - 2\beta))\text{YB}_2(\beta, \alpha, \gamma) \\
& + n(n + 1)(\phi(-\beta) - \phi(\beta))\text{YB}_3(\gamma, \alpha, \beta) \\
& + n(n + 1)(\phi(-\alpha - \beta + \pi) - \phi(-\alpha + \beta - \pi))\text{YB}_2(\alpha, \beta, \gamma) = 0
\end{aligned} \tag{A.8}$$

$$\begin{aligned}
& (\phi(-\beta)(\phi(\pi) + \phi(3\pi) - n\phi(-3\pi) + n\phi(3\pi)) - \phi(\beta)(\phi(-5\pi) + \phi(-\pi)))\text{YB}_5(\alpha, \gamma, \beta) \\
& + n(n + 1)(\phi(-2\beta) - 1)\text{YB}_2(\beta, \alpha, \gamma) \\
& - (n + 1)(\phi(-\beta - \pi) - \phi(\beta - \pi))\text{YB}_3(\gamma, \alpha, \beta) \\
& - (n + 1)(\phi(-\alpha - \beta) - \phi(-\alpha + \beta - 2\pi))\text{YB}_2(\alpha, \beta, \gamma) = 0
\end{aligned} \tag{A.9}$$

Then we eliminate  $\text{YB}_3$  from (A.7) and (A.8) to obtain

$$\begin{aligned}
& (n + 1)(\phi(\pi) + n\phi(-\pi))(\phi(-\beta) - \phi(\beta))\text{YB}_2(\beta, \alpha, \gamma) \\
& + (-n\phi(-4\pi) + n\phi(-2\pi) - \phi(2\pi) + 1)\text{YB}_5(\alpha, \gamma, \beta) = 0
\end{aligned} \tag{A.10}$$



whereas eliminating  $YB_3$  from (A.8) and (A.9) gives

$$(n-1)(n+1)(\phi(-\beta) - \phi(\beta))YB_2(\beta, \alpha, \gamma) + (-n\phi(-3\pi) + n\phi(3\pi) - \phi(-\pi) + \phi(\pi))YB_5(\alpha, \gamma, \beta) = 0 \quad (\text{A.11})$$

From (A.10) and (A.11) we can eliminate  $YB_2$ ,

$$(n\phi(-2\pi) - n\phi(2\pi) + \phi(-4\pi) + \phi(-2\pi) - \phi(2\pi) - \phi(4\pi))YB_5(\alpha, \gamma, \beta) = 0 \quad (\text{A.12})$$

Since the prefactor is not identically zero,

$$YB_5(\alpha, \beta, \gamma) = 0$$

Back-substituting, in succession, into (A.11), (A.8), the expressions for  $YB_4$  and  $YB_1$ , and (A.6), we successively obtain

$$YB_2(\alpha, \beta, \gamma) = 0$$

$$YB_3(\alpha, \beta, \gamma) = 0$$

$$YB_4(\alpha, \beta, \gamma) = 0$$

$$YB_1(\alpha, \beta, \gamma) = 0$$

$$YB_6(\alpha, \beta, \gamma) = 0$$

that is, the Yang-Baxter equations are satisfied.

## References

- [1] Smirnov S 2010 Conformal invariance in random cluster models. I. Holomorphic fermions in the Ising model *Ann. of Math.* **172** 1435–1467
- [2] Smirnov S 2010 Discrete complex analysis and probability *Proc. Int. Congr. Math.* 595–621
- [3] Chelkak D, Hongler C and Izyurov K 2012 Conformal invariance of spin correlations in the planar Ising model arXiv:1202.2838
- [4] Hongler C and Smirnov S 2013 The energy density in the planar Ising model *Acta Math.* **211** 191–225
- [5] Chelkak D and Smirnov S 2012 Universality in the 2D Ising model and conformal invariance of fermionic observables *Inventiones mathematicae* **189** 515–580
- [6] Duminil-Copin H and Smirnov S 2012 The connective constant of the honeycomb lattice equals  $\sqrt{2 + \sqrt{2}}$  *Ann. of Math.* **175** 1653–1665
- [7] Beaton NR, Bousquet-Melou M, de Gier J, Duminil-Copin H and Guttmann AJ 2014 The critical fugacity for surface adsorption of self-avoiding walks on the honeycomb lattice is  $1 + \sqrt{2}$  *Comm. Math. Phys.* **326** 727–754
- [8] Beaton NR 2014 The critical surface fugacity of self-avoiding walks on a rotated honeycomb lattice *J. Phys. A* **47** 075003
- [9] Baxter RJ 1982 *Exactly solved models in statistical mechanics* (Academic Press, London)
- [10] Riva V and Cardy J 2006 Holomorphic parafermions in the Potts model and stochastic Loewner evolution *J. Stat. Mech* P12001
- [11] Rajabpour MA and Cardy J 2007 Discretely holomorphic parafermions in lattice  $\mathbf{Z}_N$  models *J. Phys. A* **40** 14703–14713
- [12] Ikhlef Y and Cardy J 2009 Discretely holomorphic parafermions and integrable loop models *J. Phys. A* **42** 102001
- [13] Ikhlef Y 2012 Discretely holomorphic parafermions and integrable boundary conditions *J. Phys. A* **45** 265001

- [14] de Gier J, Lee A and Rasmussen J 2013 Discrete holomorphicity and integrability in loop models with open boundaries *J. Stat. Mech.* P02029
- [15] Alam IT and Batchelor MT 2012 Integrability as a consequence of discrete holomorphicity: the  $\mathbb{Z}_N$  model *J. Phys. A* **45** 494014
- [16] Fateev VA and Zamolodchikov AB 1982 Self-dual solutions of the star-triangle relations in  $\mathbf{Z}_N$ -models *Phys. Lett. A* **92** 37–39
- [17] Drinfel'd VG 1988 Quantum groups *J. Sov. Math.* **41** 898–915
- [18] Ikhlef Y, Weston R, Wheeler M and Zinn-Justin P 2013 Discrete holomorphicity and quantized affine algebras *J. Phys. A* **46** 265205
- [19] Bernard D and Felder G 1991 Quantum group symmetries in two-dimensional lattice quantum field theory *Nucl. Phys. B* **365** 98–120
- [20] Baxter RJ 1978 Solvable eight-vertex model on an arbitrary planar lattice *Philos. Trans. R. Soc. A* **289** 315–346
- [21] Lis M 2013 The fermionic observable in the Ising model and the inverse Kac-Ward operator arXiv:1303.3017
- [22] Kac M and Ward JC 1952 A combinatorial solution of the two-dimensional Ising model *Phys. Rev.* **88** 1332–1337
- [23] Fortuin CM and Kasteleyn PW 1972 On the random-cluster model: I. Introduction and relation to other models *Physica* **57** 536–564
- [24] Baxter RJ, Kelland SB and Wu FY 1976 Equivalence of the Potts model or Whitney polynomial with an ice-type model *J. Phys. A* **9** 397–406
- [25] Temperley HNV and Lieb EH 1971 Relations between the ‘percolation’ and ‘colouring’ problem and other graph-theoretical problems associated with regular planar lattices: some exact results for the ‘percolation’ problem *Proc. R. Soc. A.* **322** 251–280
- [26] Kim D and Pearce PA 1987 Scaling dimensions and conformal anomaly in anisotropic lattice spin models *J. Phys. A* **20** L451–L456
- [27] Duffin RJ 1968 Potential theory on a rhombic lattice *J. Combinatorial Theory* **5** 258–272,
- [28] Kenyon R and Schlenker JM 2005 Rhombic embeddings of planar quad-graphs *Trans. Amer. Math. Soc.* **357** 3443–3458
- [29] Costa-Santos R 2006 Geometrical aspects of the  $\mathbb{Z}$ -invariant Ising model *Eur. Phys. J. B* **53** 85–90
- [30] Bazhanov VV, Mangazeev VV and Sergeev SM 2007 Faddeev–Volkov solution of the Yang–Baxter equation and discrete conformal symmetry *Nucl. Phys. B* **784** 234–258
- [31] Nienhuis B 1990 Critical and multicritical  $O(n)$  models *Physica A* **163** 152–157
- [32] Cardy J 2009 Discrete holomorphicity at two-dimensional critical points *J. Stat. Phys.* **137** 814–824